Article

Vacuum Die Casting Process and Simulation for Manufacturing 0.8 mm-Thick Aluminum Plate with Four Maze Shapes

Chul Kyu Jin [1], Chang Hyun Jang [1] and Chung Gil Kang [2,*]

[1] Graduate School of Mechanical and Precision Engineering, Pusan National University, San 30 Chang Jun-dong, Geum Jung-Gu, Busan 609-735, Korea;
E-Mails: ckjeans82@pusan.ac.kr (C.K.J.); jangch@hyundai-wisco.com (C.H.J.)

[2] School of Mechanical Engineering, Pusan National University, San 30 Chang Jun-dong, Geum Jung-Gu, Busan 609-735, Korea

* Author to whom correspondence should be addressed; E-Mail: cgkang@pusan.ac.kr;
Tel.: +82-51-510-1455; Fax: +82-51-518-1456.

Abstract: Using vacuum die casting, 0.8 mm-thick plates in complicated shapes are manufactured with the highly castable aluminum alloy Silafont-36 (AlSi9MgMn). The sizes and shapes of the cavities, made of thin plates, feature four different mazes. To investigate formability and mechanical properties by shot condition, a total of six parameters (melt temperatures of 730 °C and 710 °C; plunger speeds of 3.0 m/s and 2.5 m/s; vacuum pressure of 250 mbar and no vacuum) are varied in experiments, and corresponding simulations are performed. Simulation results obtained through MAGMA software show similar tendencies to those of the experiments. When the melt pouring temperature is set to 730 °C rather than 710 °C, formability and mechanical properties are superior, and when the plunger speed is set to 3.0 m/s rather than to 2.5 m/s, a fine, even structure is obtained with better mechanical properties. The non-vacuumed sample is half unfilled. The tensile strength and elongation of the sample fabricated under a melt temperature of 730 °C, plunger speed of 3.0 m/s, and vacuum pressure of 250 mbar are 265 MPa and 8.5%, respectively.

Keywords: vacuum die-casting; thin plate; aluminum alloy; casting simulation; casting defects

1. Introduction

Many industries, including the automobile, aircraft, and electronics sectors, have actively researched replacing ferrous alloys with light alloy materials, such as aluminum and magnesium. Replacing a ferrous alloy with a light alloy degrades mechanical properties and increases costs, which are large problems in these industries. The density of aluminum (2.7 g/cm^3) is one-third that of iron (7.9 g/cm^3) and, as its mechanical properties and workability are excellent, aluminum is used for casting and forging. Even with these advantages, because an aluminum alloy has substantially inferior mechanical properties compared with those of a ferrous alloy, alloy composition and process methods should be improved for better mechanical properties [1–6].

Aluminum process methods are classified into casting, forging, and plastic deformation. Die-casting is a method that produces a product by pouring melt into a mold followed by punch-pressing, which allows a complicated shape to be fabricated. However, because die-casting injects melt at a high velocity, gases and air remaining in the melt may cause internal defects; therefore, the product's mechanical properties are degraded. An enhanced die-casting method, vacuum die-casting, has been developed by adding a vacuum device. Because vacuum die casting creates a vacuum inside the mold cavity during casting, gases or air in the melt is removed, decreasing the volume of gas pockets and improving the mechanical properties and smoothness of the resulting surface [7,8]. Using an aluminum or magnesium alloy made by vacuum die-casting, aircraft and automotive parts in bulk shapes have been manufactured. Recently, studies on manufacturing 0.8-mm-thick, thin-plated products have been introduced [9–12].

When manufacturing a thin-plated part, the fluidity of a material is extremely important, so a casting alloy with 10% silicon content needs to be used. Moreover, it is necessary to analyze the behavior of melt when it is poured into a mold and fills the cavity, and to predict regions in which the flow of the melt is not smooth or unstable and casting defects occur. For this process, filling and solidification analyses need to be conducted by using computer-aided engineering (CAE).
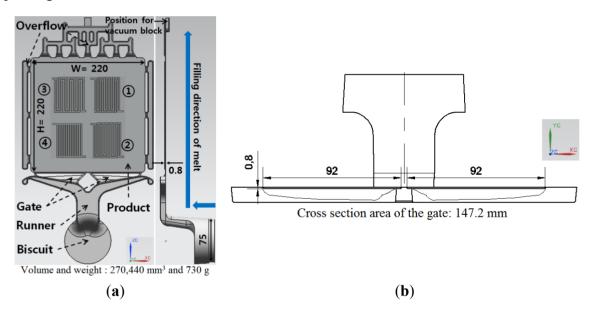
In this study, we propose a method for manufacturing a thin aluminum plate with a complicated shape by using vacuum die-casting. The shape of the mold cavity with four mazes is complex and the thickness of the mold is 0.8 mm. Using CAE, the behavior of the melt and any defects are predicted, which are then compared against the actual results of an experiment. Then, the formability of a thin plate in accordance with shot conditions and mechanical properties of the manufactured plates are comparatively analyzed. For the experiment, a 660-ton cold chamber die-casting machine was used and the melt material was a Silafont-36 (AlSi9MgMn) alloy.
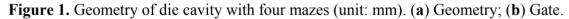
2. Experimental Section

2.1. Mold Design

Figure 1a presents an image of the cavity in the vacuum die casting mold. The mold structure for vacuum die casting consists of a biscuit, a runner, gates, a product, and overflows. The melt is poured into the biscuit and filled to the product after passing through the runner and gates. Because the behavior of the melt filled into the product is highly affected by the shape of the gates, designing a gate appropriate for the shape of the product is essential. A gate has an appropriate shape for a thin plate. Melt injected through a gate can fill the cavity in sequence up to the overflows [10,11,13–15].

The overflows are the parts where the melt is filled last and should be located at the position where material filling is incomplete; these are located on the left and right of the product and on the other side of the gate, which is the last region to be filled by the melt. The vacuum block is located at the end of the overflow on the other side of the gate. The valve opens during filling and it is closed by the pressure of the melt. The shape of the product is a thin plate with four mazes. In size the product is 220 mm high, 220 mm wide, and 0.8 mm thick. Figure 1b shows the cross section of a gate. The cross-sectional area of the gate connected with the product is 147.2 mm. Figure 2 presents plane and sectional images of the four mazes. The four mazes are shaped as squares with 0.3 mm-deep grooves and different paths in each maze. Mazes 1 and 4 are 41 mm wide and 58 mm high with the same 0.9-mm-wide grooves, but the maze shapes are different (Maze 1 is serpentine and Maze 4 is straight). Maze 2 is 45 mm wide and 58 mm high with 1.0-mm-wide grooves; its shape is serpentine, the same as that of Maze 1. Maze 4 is 45 mm wide and 58 mm high with 1.2-mm-wide grooves; its shape is serpentine, the same as those of Mazes 1 and 3. The thickness of the four mazes is 1.1 mm, including the depth of grooves, which is 0.3 mm.
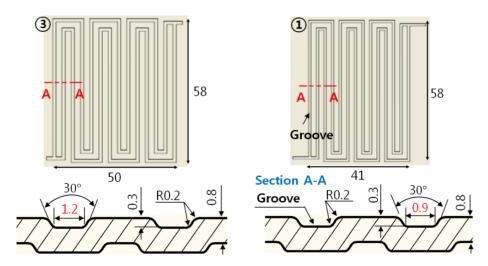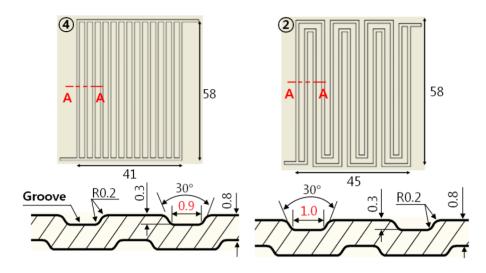

(**a**)

(**b**)

Figure 1. Geometry of die cavity with four mazes (unit: mm). (**a**) Geometry; (**b**) Gate.

Figure 2. *Cont.*

Figure 2. Detail view of four mazes (unit: mm): ① maze 1; ② maze 2; ③ maze 3 and ④ maze 4.

2.2. Conditions of the Experiment and Simulation

The casting simulation was performed using the MAGMA 5.1 software (MAGMA Giessereitechnologie GmbH, Aachen, Germany), set according to the melt temperature, plunger speed, and vacuum pressure. MAGMA's mesh-partitioning method is the finite volume method (FVM). An accurate simulation result requires at least three meshes per axis. Because too many meshes would require a substantial amount of time for calculation, an appropriate number of meshes needs to be determined. Accordingly, to generate three meshes in the direction of the plate's thickness, meshes were divided as much as possible in the *y*-axis, which is the direction of the thickness. The results were 594,275 meshes on the metal cell (cast) and 14,575,210 meshes on the control volume, which is the material group (mold) as shown in Figure 3. All other conditions in the simulation were determined to be the same as those of the experiment.
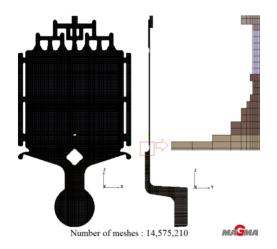

Figure 3. Mesh of die cavity with four mazes (unit: mm).

A 660-ton Buhler cold chamber die casting process was used for the shot experiment. In this process, the melt is poured into the sleeve, and the plunger inside the sleeve pushes the melt into the mold. The length of the shot sleeve is 470 mm and the diameter of the plunger is 75 mm. Figure 4 shows the vacuum die casting process. During the first process of vacuum die-casting, a vacuum pump

creates a vacuum inside the mold cavity. The melt is injected through the pouring hole in the shot sleeve, and the plunger pushes it into the mold. The plunger moves at a low speed (V_1) up to a point 400 mm inside the sleeve and at a high speed (V_2) between the points 400 mm and 470 mm into the sleeve. As soon as the plunger reaches the point of 470 mm, it pressurizes the melt at 500 bar; this is when the melt solidifies in the cavity, forming into a product. Filling time is about 327 ms during which melt moves from the chamber to the overflow. It only takes about 12 ms to completely fill the die cavity. Table 1 presents the parameters of the vacuum die casting process, and Table 2 lists the shot conditions (experimental). We examined the effects of melt temperature, plunger speed, and vacuum pressure on formability and mechanical properties. The temperatures of the pouring melt were 710 °C and 730 °C, and the vacuum pressures were 250 mbar and no vacuum. The plunger speeds were 0.2 m/s for the low speed (V_1) and 2.5 and 3.0 m/s for the high speeds (V_2). As Table 2 shows, there were a total of six shot conditions, and each condition was tested five times. To eliminate variation of fluid characteristics of the melt attributable to the mold's changing temperature, five preparatory shots were made prior to the actual shots, maintaining the temperature of the mold at 250 °C. The melt was the die-casting alloy Silafont-36 (AlSi9MgMn). A Silafont-36 material has 10% Si content and has an excellent castability along with superior weldability and workability. Further, the Fe content of this die-casting alloy is less than 0.13% in Mn content, preventing the mold from sticking and improving mechanical properties (e.g., high ductility) owing to the Mg content [16,17]. The alloy composition of Silafont-36 is presented in Table 3.
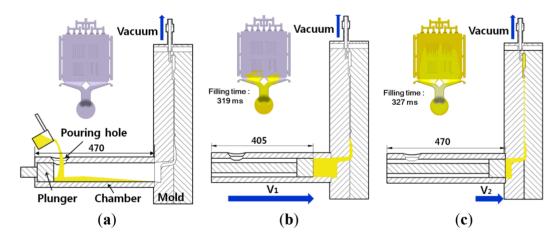

Figure 4. Vacuum die casting process: (**a**) Input melt in chamber; (**b**) Slow shot and (**c**) Fast shot.

Table 1. Process parameters of vacuum cold chamber die-casting.

	Parameters	Values
Melt	Material	Silafont-36
	Pouring Temperature (T_m)	710, 730 °C
Die	Material	SKD 61
	Temperature	250 °C
Length of shot sleeve		470 mm
Length at low (V_1) and high (V_2) speed		400 and 70 mm
Working pressure		500 bar
Heat transfer coefficients	between material and mold	3000 W/m^2·K
	between mold and mold	1000 W/m^2·K

Table 2. Experimental conditions of vacuum cold chamber die-casting.

No	T_m (°C)	V_1 (m/s)	V_2 (m/s)	Vacuum (mbar)
1	700	0.2	2.5	250
2	700	0.2	3.0	no vacuum
3	700	0.2	3.0	250
4	730	0.2	2.5	250
5	730	0.2	3.0	no vacuum
6	730	0.2	3.0	250

Table 3. Chemical composition of Silafont-36 alloy (wt. %).

Si	Mn	Mg	Ga	Ti	Fe
9.91	0.662	0.372	0.011	0.07	0.07

Zn	Cr	Cu	Ca	Al
0.002	0.001	0.001	0.0005	Bal

3. Results and Discussion

3.1. Formability

Figure 5 presents samples, fabricated of thin plates, under the six shot conditions listed in Table 2. Each of the shot conditions was tested five times, producing to a total of 30 samples. Figure 5 shows a selection of the best samples from each condition. As Figure 5 indicates, the product area in each sample was incompletely filled. The six samples were all unfilled in the mazes and, in particular, Mazes 1 and 3, positioned at the end of the product area, were unfilled. While the melt passed through the bumps in the front-positioned Mazes 2 and 4, its fluidity substantially decreased and turbulence occurred. We conclude that the unstable turbulence caused a sudden solidification through Mazes 1 and 3. Of the six conditions, the best formability was found under Condition 6 (T = 730 °C, V_2 = 3.0 m/s, P_{vacuum} = 250 mbar), and the sample fabricated under this condition was unfilled only at the end of the product area and where the overflows were connected.

Better formability was found when the melt pouring temperature was 730 °C rather than 710 °C. Figure 6 presents simulation results (for varying filling temperature) for Conditions 3 and 6 with pouring temperatures of 710 °C and 730 °C, respectively, when the plunger speed was 3.0 m/s and the vacuum pressure was 250 mbar. The simulation result presents the temperature distributions immediately after the melt filled 88% and 100% of the cavity. In Figure 6a, when the pouring temperature of the melt was set to 730 °C, the temperature remained at approximately 725 °C from the gate to the entrances of Mazes 2 and 4. The temperature at the center of the product was roughly 722 °C, and from the ends of Mazes 1 and 3 to the entrances of the overflows the melt solidified rapidly and temperatures remained at approximately 715 °C. The parts at which the temperature rapidly dropped were more likely unfilled, as the fabricated samples show in Figure 5. Figure 6b presents a simulation result when the melt temperature was set to 710 °C. The front half of the product (from the gate to the entrances of Mazes 1 and 3) is at roughly 702 °C, and the other half (from the entrances of Mazes 1 and 3 to the overflows) is at 698 °C. This result suggests that the back half of a product is more likely to remain unfilled. In addition, because there are parts in Mazes and at the entrance of the overflow at which

rapid solidification occurs at 700 °C and 695 °C, respectively, it is possible that the mazes could be partially unfilled. The image of the sample (Condition 3) presented in Figure 5, shows a similar result to that of the simulation. Approximately 2 mm at the ends of Mazes 2 and 4 was unfilled. Mazes 1 and 3 contain many unfilled regions, sized 2 mm and over 5 mm. The back half of the products had flow marks, indicating that the melt flow was very unstable.
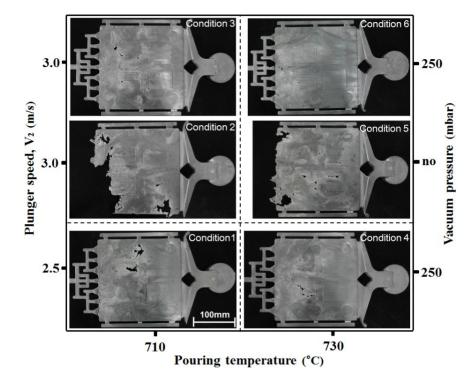

Figure 5. Samples fabricated by vacuum die casting with different parameters: Condition 1 (T = 710 °C, V_2 = 2.5 m/s, P_{vacuum} = 250 mbar); Condition 2 (T = 710 °C, V_2 = 3.0 m/s, no vacuum); Condition 3 (T = 710 °C, V_2 = 3.0 m/s, P_{vacuum} = 250 mbar); Condition 4 (T = 730 °C, V_2 = 2.5 m/s, P_{vacuum} = 250 mbar); Condition 5 (T = 730 °C, V_2 = 3.0 m/s, no vacuum); Condition 6 (T = 730 °C, V_2 = 3.0 m/s, P_{vacuum} = 250 mbar).
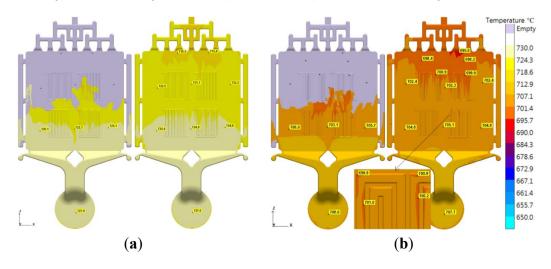

Figure 6. Temperature distribution in die cavity with different pouring temperatures during vacuum die-casting: (**a**) 730 °C and (**b**) 710 °C.

For the plunger speed parameter, *i.e.*, the speed of the plunger's travel, better formability was found at 3.0 m/s than at 2.5 m/s. Figure 7 presents simulation results for Conditions 6 and 4, with plunger speeds of 3.0 m/s and 2.5 m/s, respectively, when the melt temperature was 730 °C and the vacuum pressure was 250 mbar. The simulation results show velocity distributions and gas content immediately after the melt filled the cavity. In Figure 7a, showing Condition 6 with a plunger speed of 3.0 m/s, the velocity distribution of the melt remained constant at 82–90 m/s throughout the product area and was 83 m/s on the left and right edges and in the gap between the mazes. In Mazes 2 and 1 the velocity of the melt was 32 m/s and 36 m/s, respectively and in Mazes 4 and 3 it was 56 m/s and 23 m/s, respectively. This result indicates that the melt substantially slowed as it passed the bumps of the mazes. Under Condition 4 (Figure 7b), when the plunger speed was set to 2.5 m/s, the entire product area indicated approximately 67–81 m/s. Moreover, in the mazes the velocity decreased more than under Condition 6. In Mazes 2 and 1 the velocity of the melt was 24 m/s and 21 m/s, respectively, and in Mazes 4 and 3 it was 50 m/s and 30 m/s, respectively. It is predicted that the melt solidifies while passing through the mazes. The result in terms of air entrapment, indicating gas content in the cavity, shows that the higher the air entrapment, the more unstable the fluid flow in the cavity and the higher the chance of air pockets in the product. As the air entrapment results suggest under these two conditions, air entrapment was high from the ends of Mazes 1 and 3 to the entrances of overflows. In Condition 4, air entrapment was high in the mazes; Mazes 1 and 3, in particular, showed substantial air entrapments. As the fabricated sample images in Figure 5 suggest, Mazes 1 and 3 under Condition 4 had unfilled parts and hot tears in the product area. The flow marks indicate that the melt flow was extremely unstable while passing through Mazes 2 and 4.

Under Conditions 2 and 5, in which no vacuum was used, unfilled parts were found throughout the product and the overflows in the ends were completely unfilled. This result suggests that vacuum is an important factor, substantially affecting formability (castability) in the fabrication of a thin plate in the die-casting process.
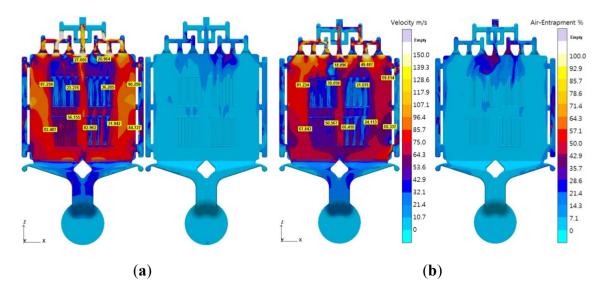

Figure 7. Velocity distribution of the melt and air content in the die cavity using different plunger speeds in vacuum die-casting: (**a**) 3.0 m/s and (**b**) 2.5 m/s.

3.2. Microstructures and Mechanical Properties

Each fabricated sample was examined for its microstructure and mechanical properties. To observe the microstructure of a sample, a 10 × 10 mm cut was made from the center of a specimen, mounted and polished, and observed using an optical microscope. To assess mechanical properties, tensile and Vickers hardness tests were performed. For the tensile test, rectangular tension test specimens (subsize specimens) were prepared according to ASTM E8M with gage length and width of 25 mm and 6 mm, respectively. The thickness of the tensile specimens was the same as that of the fabricated thin plate samples. The tensile test was performed at 25 ton MTS, and the strain rate was 1 mm/min. The tensile specimens were cut with a gap between the gate and Mazes 2 and 4. For the measurement of Vickers hardness, the specimens for microstructure assessment were used. Each specimen was tested five times for hardness; the results were averaged (symbol: ■) and the maximum and minimum are also presented.

Figure 8 shows microstructures of the samples fabricated under all conditions. Table 4 shows the grain size of the primary α-Al phase. In the microstructures, the white parts indicate the primary α-Al phase and the remaining parts indicate the eutectic phase; the black parts indicate air pockets. The primary α-Al phase in the microstructure of the sample, fabricated at a melt temperature of 730 °C, was coarser than that fabricated at 710 °C, which indicates that its primary α-Al phase was coarser because the pouring temperature of 730 °C required more time to solidify than that of 710 °C. For the plunger speed, the microstructure of the sample fabricated at 3.0 m/s has more primary α-Al phases than that at 2.5 m/s; when the plunger speed was set to 3.0 m/s rather than 2.5 m/s, the melt more evenly and stably filled the cavity. The vacuumed samples had some porosity whereas the non-vacuumed ones had many gas pockets, indicating that vacuum operation is excellent for removing gases from the cavity and the melt. If the primary α-Al phase is coarse or irregular in shape, the hardness decreases; because the primary α-Al phase is soft, less primary α-Al phase also decreases the ductility. A large degree of porosity easily causes cracks and degrades mechanical properties. The microstructure of the sample fabricated under Condition 6 showed the most even distribution. The mix of the primary α-Al and eutectic phases was properly fractional, and the equivalent diameter in the primary α-Al phase was 74 μm in size and generally spherical.

To measure the porosity of samples formed under vacuum the blister test was conducted. Samples formed without vacuum were excluded due to many defects. Maze 1 was prepared for the blister test and heat-treated at 520 °C for five hours. Figure 9 shows the appearance of samples after the blister test. The red areas represent blister defects. Samples fabricated under Conditions 1 and 4 at a melt temperature of 710 °C have some blisters. In the case of Conditions 3 and 6 fabricated at a melt temperature of 730 °C, the Condition 6 sample has only one blister and the Condition 3 sample has no blisters.
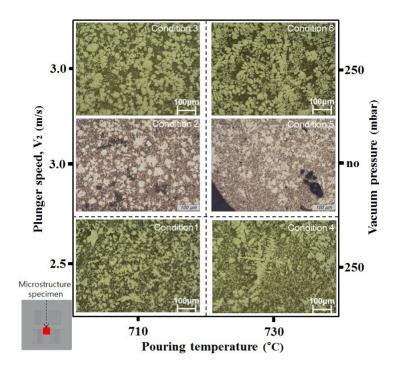
Figure 8. Microstructures of samples fabricated by vacuum die casting with different parameters: Condition 1 (T = 710 °C, V_2 = 2.5 m/s, P_{vacuum} = 250 mbar); Condition 2 (T = 710 °C, V_2 = 3.0 m/s, no vacuum); Condition 3 (T = 710 °C, V_2 = 3.0 m/s, P_{vacuum} = 250 mbar); Condition 4 (T = 730 °C, V_2 = 2.5 m/s, P_{vacuum} = 250 mbar); Condition 5 (T = 730 °C, V_2 = 3.0 m/s, no vacuum); Condition 6 (T = 730 °C, V_2 = 3.0 m/s, P_{vacuum} = 250 mbar).

Table 4. Grain size of primary α-Al phase.

Condition	1	4	2
Size	70	80	70
Condition	**5**	**3**	**6**
Size	68	71	74

Figure 10 presents the tensile strengths, elongations, and Vickers hardness values of the samples made under all conditions. For Conditions 2 and 5 without vacuum operation, the tensile strengths of the samples were 180–185 MPa; the elongations were 4%–5%; and Vickers hardnesses were 78–79 HV. These results are very different from those under vacuum conditions. The mechanical properties among the vacuum samples varied little. As for the effects of the melt pouring temperatures, Conditions 4 and 6 when the temperature was 730 °C showed better mechanical properties than those at 710 °C: tensile strengths were higher by 5–7 MPa, elongations were higher by 0%–1%, and Vickers hardnesses were higher by 3 HV. The primary α-Al phase of the sample fabricated at a melt temperature of 730 °C was coarser than that at 710 °C; on the other hand, the tensile strength, elongation, and hardness of the samples fabricated at 730 °C were higher than those at 710 °C. The reason for this is that samples fabricated at 710 °C have more porosities than those at 730 °C, as shown in Figure 9. For the plunger speed set to 3.0 m/s under Conditions 3 and 6, tensile strengths were higher by 8–10 MPa, elongations longer by 1.5%–2.5%, and Vickers hardnesses higher by 2 HV than those under Conditions 1 and 4 when plunger speed was set to 2.5 m/s. This is because samples

fabricated at 3.0 m/s have more of the primary α-Al phase than samples at 2.5 m/s. In addition, the primary α-Al phase of sample fabricated at 2.5 m/s was more irregular in shape than for samples at 3.0 m/s. Therefore, the effect of plunger speed on the mechanical properties was greater than that of melt temperature. The mechanical properties of Condition 6, which displayed good formability and the most evenly distributed microstructure compared to the other samples, were the superior. Its tensile strength and elongation were 265 MPa and 8.5%, respectively, and its Vickers hardness was 105 HV.

Figure 9. Appearance of samples after blister test (490 °C, five hours): (**a**) Condition 3 (T = 710 °C, V_2 = 3.0 m/s); (**b**) Condition 6 (T = 730 °C, V_2 = 3.0 m/s); (**c**) Condition 1 (T = 710 °C, V_2 = 2.5 m/s) and (**d**) Condition 4 (T = 730 °C, V_2 = 2.5 m/s). The red areas represent blister defects.
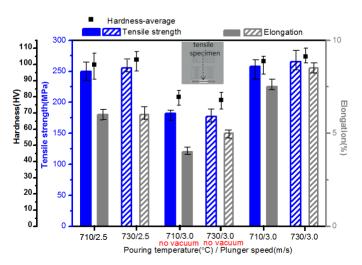

Figure 10. Mechanical properties of samples fabricated by vacuum die casting with different parameters.

The maze part of the sample fabricated under Condition 6 was cut, and its surface and cross section were measured with a digital microscope. Figure 11a presents the surface at 40× magnification and Figure 11b presents the cross section. As the cross section shows, the thicknesses ranged between 0.77 mm and 0.79 mm and the depths of the groves ranged between 0.31 mm and 0.36 mm.
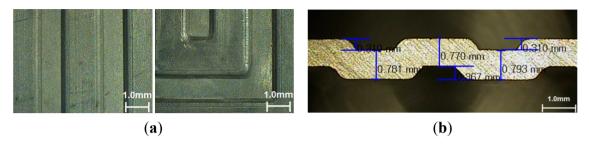

(**a**) (**b**)

Figure 11. Surface and cross section in Maze 4 of a sample fabricated with a pouring temperature of 730 °C, plunger speed of 3.0 m/s, and vacuum pressure of 250 mbar (40× magnification). (**a**) Surface; (**b**) Cross section.

4. Conclusions

Using vacuum die casting with a Silafont-36 alloy, we fabricated a thin plate into samples with complex shapes containing four mazes. Findings in terms of formability and mechanical properties of samples fabricated under different melt temperature, plunger, and vacuum pressure values are summarized as follows: (1) When the melt filled the cavity, its fluidity substantially decreased and turbulence occurred while it passed over bumps in the mazes near the gate. The turbulence of the melt caused rapid solidification as it passed through the next mazes, which were partially unfilled. (2) None of the six shot conditions produced a perfect filling. However, the sample fabricated under a melt temperature of 730 °C, plunger speed of 3.0 m/s, and vacuum pressure of 250 mbar was completely filled except for the end of the product and the places where overflows were connected. (3) The microstructure of the sample fabricated at a melt temperature of 730 °C was coarser in the primary α-Al phase than in the sample fabricated at 710 °C. The microstructure of the sample formed at a plunger speed of 3.0 m/s displayed more primary α-Al phase than in the sample formed at 2.5 m/s. The non-vacuumed sample contained many air pockets. (4) The tensile strength and elongation of the sample fabricated at a melt temperature of 730 °C were higher than for those at 710 °C by 6 MPa and 0.5%, respectively. The tensile strength and elongation of the samples fabricated at a plunger speed of 3.0 m/s were higher than for those fabricated at 2.5 m/s by 9 MPa and 2%, respectively. The tensile strength and elongation of the non-vacuumed sample were lower than those of the samples formed under other conditions by approximately 74.5 MPa and 2.5%, respectively. Therefore, it appears that vacuum pressure strongly affects formability and mechanical properties, and that plunger speed rather than melt temperature is the factor that more strongly affects mechanical properties. (5) The tensile strength and elongation of the sample fabricated under a melt temperature of 730 °C, plunger speed of 3.0 m/s, and vacuum pressure of 250 mbar were 265 MPa and 8.5%, respectively.

Acknowledgments

Author Contributions

Chu Kyu Jin designed die of vacuum die casting by performing the simulation. Chul Kyu Jin and Chang Hyun Jang conducted shot experiment and analysis the results. Chung Gil Kang maintained and examined the results of simulation and experiment. All authors have contributed to discussing and revising.

Conflicts of Interest

The authors declare no conflict of interests.

References

1. Lee, K.H.; Kwon, Y.N.; Lee, S.H. Correlation of microstructure with mechanical properties and fracture toughness of A356 aluminum alloys fabricated by low-pressure-casting, rheo-casting, and casting-forging processes. *Eng. Fract. Mech.* **2008**, *75*, 4200–4216.
2. Birol, Y. Semi-solid processing of the primary aluminium die casting alloy A365. *J. Alloys Compd.* **2009**, *473*, 133–138.
3. Atkinson, H.V. Modelling the semisolid processing of metallic alloys. *Prog. Mater. Sci.* **2005**, *50*, 341–412.
4. Dørum, C.; Laukli, H.I.; Hopperstad, O.S.; Langseth, M. Structural behaviour of Al-Si die-castings: Experiments and numerical simulations. *Eur. J. Mech. A Solids* **2009**, *28*, 1–13.
5. Fan, Z.; Fang, X.; Ji, S. Microstructure and mechanical properties of rheo-diecast (RDC) aluminium alloys. *Mater. Sci. Eng. A* **2005**, *412*, 298–306.
6. Miller, A.E.; Maijer, D.M. Investigation of erosive-corrosive wear in the low pressure die casting of aluminum A356. *Mater. Sci. Eng. A* **2006**, *435–436*, 100–111.
7. Niu, X.P.; Hu, B.H.; Pinwill, I.; Li, H. Vacuum assisted high pressure die casting of aluminium alloys. *J. Mater. Process. Technol.* **2000**, *105*, 119–127.
8. Kim, E.S.; Lee, K.H.; Moon, Y.H. A feasibility study of the partial squeeze and vacuum die casting process. *J. Mater. Process. Technol.* **2000**, *105*, 42–48.
9. Kim, Y.C.; Kang, C.S.; Cho, J.I.; Jeong, C.Y.; Choi, S.W.; Hong, S.K. Die casting mold design of the thin-walled aluminum case by computational solidification simulation. *J. Mater. Sci. Technol.* **2008**, *24*, 383–388.
10. Jin, C.K.; Kang, C.G. Fabrication process analysis and experimental verification for aluminum bipolar plates in fuel cells by vacuum die-casting. *J. Power Sour.* **2011**, *196*, 8241–8249.

11. Jin, C.K.; Kang, C.G. Fabrication by vacuum die casting and simulation of aluminum bipolar plates with micro-channels on both sides for proton exchange membrane (PEM) fuel cells. *Int. J. Hydrog. Energy* **2012**, *37*, 1661–1676.

12. Cho, C.Y.; Uan, J.Y.; Lin, H.J. Surface compositional inhomogeneity and subsurface microstructures in a thin-walled AZ91D plate formed by hot-chamber die casting. *Mater. Sci. Eng. A* **2005**, *402*, 193–202.

13. Hu, B.H.; Tong, K.K.; Niu, X.P.; Pinwill, I. Design and optimisation of runner and gating systems for the die casting of thin-walled magnesium telecommunication parts through numerical simulation. *J. Mater. Process. Technol.* **2000**, *105*, 128–133.

14. Jin, C.K.; Bolouri, A.; Kang, C.G.; Hwang, G.W. Thin-plate forming by thixo- and rheoforging. *Adv. Mech. Eng.* **2014**, *2014*, 1–12.

15. Cleary, P.W.; Ha, J.; Prakash, M.; Nguyen T. Short shots and industrial case studies: Understanding fluid flow and solidification in high pressure die casting. *Appl. Math. Model.* **2010**, *34*, 2018–2033.

16. Franke, R.; Dragulin, D.; Zovi, A.; Casarotto, F. Progress in ductile aluminium high pressure die casting alloys for the automotive industry. *Metall. Ital.* **2007**, *5*, 21–26.

17. Zovi, A.; Casarotto, F. Silafont-36, the low iron ductile die casting alloy development and applications. *Metall. Ital.* **2007**, *6*, 33–38.